Sarah K. Allawi Mohammed A. Akraa

Department of Physics, College of Education for Pure Science, University of Babylon, Al-Hilla, Babil, IRAQ



Synthesis and Characterization of Metamaterials from Beetroot Juice and Metal Salt Solutions

The study involved creating a unique metamaterial using a reproducible organometallic complex made from natural and affordable ingredients. The process included creating the material through sedimentation by adding beetroot juice to an ionic aqueous solution containing $\text{CuSO}_4.5\text{H}_2\text{O}$ and/or AgNO_3 compounds. Different weight percentages of the compounds were used (100% Cu, 80% Cu + 20% Ag, 60% Cu + 40% Ag, 40% Cu + 60% Ag, 20% Cu + 80% Ag, and 100% Ag wt.%).The material was analyzed using Differential Scanning Calorimetry (DSC), Fourier Transform Infrared spectroscopy (FTIR), and UV-Vis spectroscopy. The presence of silver ions made the sediment less stable and led to more ligand deposition, higher reflectance, and reduced absorbance and transmittance. The band gap widened with the highest value for the sample with 20% Cu + 80% Ag. Higher silver ion concentration resulted in a negative spectrum of refractive index, imaginary electric permittivity, and optical conductivity.

Keywords: Metamaterials; Organometallic complex; Optical properties; Refractive index Received: 13 July 2024; Revised: 24 August 2024; Accepted: 31 August 2024

1. Introduction

In recent decades, there have been notable advancements in the field of metamaterials. Metamaterials, which are artificially engineered structures with unique microstructures, have facilitated a wide range of applications, spanning from telecommunications to energy harvesting. Nevertheless, the synthesis of metamaterials often necessitates intricate procedures and costly raw materials, thereby posing significant challenges [1].

The manuscript introduces innovative ecofriendly meta-materials. The interesting aspect of the presented product is that originates from affordable and accessible compounds of beetroot juice and metal salt solutions. The natural dye of beetroot is rich in anthocyanin and betalain (the chemical structures of which are shown in Fig. (1). These chemical species result in superb features of light absorption and emission.

Betalain refers to a group of dyes found in numerous plants, predominantly in beetroot (Beta vulgarize). The presented natural colorants involve several vital properties. The specific chemical composition of the betalain consists of chromophores (the responsible molecular parts for appearing color) coupled to the molecule of sugar. The attached side chains contribute to the pyrrole ring structure of the chromophore [2].

Anthocyanins are a type of flavonoid that contains phenolic structures. They consist of a backbone of fifteen carbon atoms composing two aromatic rings (phenol groups) and one heterocyclic ring with an oxygen atom. These aromatic rings are constituted by phenolic compounds. The chemical structure of anthocyanins includes hydroxyl (-OH) and/or methoxyl (-OCH₃) groups, as well as one or more sugars. The presence of phenolic character in anthocyanins is due to the combination of hydroxyl groups with aromatic rings. Anthocyanins possess

antioxidant properties because of their association with phenols [2].

Fig. (1) Chemical structure of betalain and anthocyanin [2]

Concurrently, mixing the metal salts with the beetroot juice creates structured complexes due to the interaction between the metal ions in one aspect and the anthocyanin and betalain in the other aspect [3]. The unique optical properties of the product provide a simple and effective procedure for metamaterial synthesis.

Metamaterials, typically created by humans, have extraordinary properties due to their structure, not their composition. Unprecedented manipulation of electromagnetic waves, elastic waves, molecules, and particles is achievable through groundbreaking methods. Metamaterials, classified as 'left-handed' or 'double-negative' materials, exhibit negative permeability. permittivity and Mechanical metamaterial with unique microstructures, including origami, chiral, and lattice types, possess exceptional properties, such as ultra-lightweight and ultrastiffness [4].

The research aims to bridge the gap between complex synthetic procedures and the need for accessible metamaterials. The anticipated findings are poised to substantially advance the field of metamaterials and create pathways for harnessing natural resources in advanced material synthesis.

Differential scanning calorimetry (DSC) serves as a powerful tool for gaining crucial insights into metamaterials. It enables the determination of thermal stability, identification of phase transitions, estimation of purity, understanding of reaction kinetics, and measurement of specific heat capacity. Understanding these properties is imperative for diverse applications and for comprehending the behavior of metamaterials under varying conditions [5].

Researching metamaterials necessitates the application of FTIR spectroscopy, which plays a crucial role in the identification of unknown compounds, the provision of quantitative data related to additive presence, the offer of kinetic information concerning infrared absorptions, and the delivery of complex data when used in conjunction with instruments such as TGA or GC. When utilized alongside resonant nanoparticles metasurfaces, FTIR enhances detection capabilities significantly. In summary, a comprehensive understanding of the composition and behavior of metamaterials mandates the utilization of FTIR spectroscopy [6]. Metamaterial spectral analysis requires UV-Visible spectroscopy to examine their response to different light wavelengths.

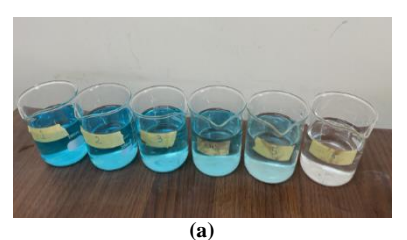
2. Materials and Method

This part included the production of the required material. The considered samples were products of adding well-filtered beetroot juice (50 mL) to the different ionic concentrations of dissolved copper sulfate pentahydrate (CuSO₄.5H₂O) and silver nitrate (AgNO₃) solution in deionized water (200 mL). The following table (1) illustrates the weight percent of the copper and silver in the used solution of the six samples.

Table (1) Weight percentages of copper and silver in the considered six samples

Sample	Weight Percent of Copper wt.%	Weight Percent of Silver wt.%
1	100	0
2	80	20
3	60	40
4	40	60
5	20	80
6	0	100

The mixtures produced by the addition process should be left for approximately 48 hours. During this time, interesting discoloration of the six samples was observed. The change in colors of the samples' solutions by the interaction of the beetroot juice with them can be seen in figures (2a) and (2b), which display the colors of the solutions before and after the interaction and extraction of the produced precipitate.



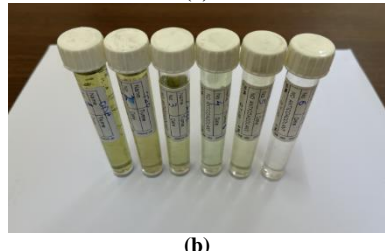


Fig. (2) (a) The aqueous solutions before adding the beetroot juice, (b) The aqueous solution after adding the beetroot juice and extraction the precipitates

The weight percent of copper and silver in one gram of CuSO₄.5H₂O and AgNO₃, are 25.45 and 63.5 wt.%, respectively. These values are calculated based on the molar masses of the elements and the compound. The reaction between the beetroot juice and the prepared ionic solution resulted in sediment forming in each of the samples. The separation process was achieved by centrifuging using a CENTERIFUGE 80-1 (China). Each centrifugation period lasted for 20 minutes at 4000 rpm. Throughout this stage of the extraction process. the precipitate was washed multiple times with deionized water and ethanol to remove any potential sugar and oil that may be present in the beetroot juice. After each washing period, the supernatant was removed for cleanliness. The extracted precipitate was left to dry for several days in an isolated chamber to prevent contamination. Additionally, the supernatant from the samples was collected in tubes for further analysis.

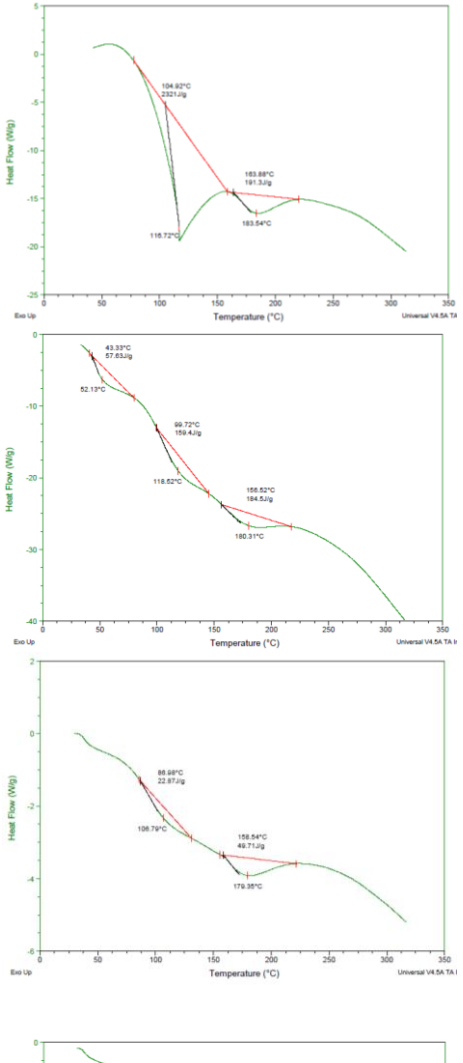
The samples' precipitate was subjected to DSC testing using a DSC Q600 (USA) apparatus to identify the product's crystalline nature and stability.

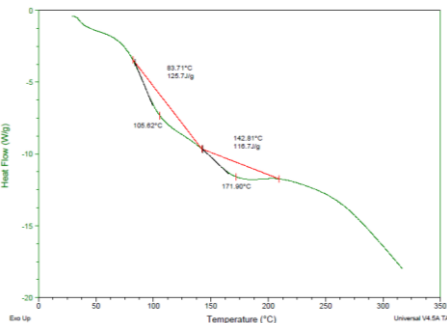
Both components of the interaction products, precipitate and supernatant, undergo FTIR analysis within a range of wavenumbers 400-4000 cm⁻¹ using a Shimadzu 1800 (Japan) Fourier-transform instrument. The process of measuring absorbance was carried out using a Shimadzu UV-2450 spectrophotometer with a spectral bandwidth of 4 nm and a broad spectrum of wavelengths 200-800nm.

3. Results and discussion

The specimens underwent DSC analysis, which measures the amount of absorbed or released heat flow of the tested material. All the specimens exhibited two peaks with downward points, except for specimen two, which showed three peaks with downward points, indicating an endothermic reaction [7]. Figure (3) illustrates the behavior of the

six samples as the temperature rose from approximately 50 to 300°C. The first onset point of each specimen's first downward peak marks the temperature at which the curve deviates from the baseline (the red line representing no thermal event). The glass transition point occurs at a lower temperature than the melting point, marked by the second onset point of the second downward peak on each DSC analysis chart. The lowest temperature of each curve represents the average transition temperature [7].





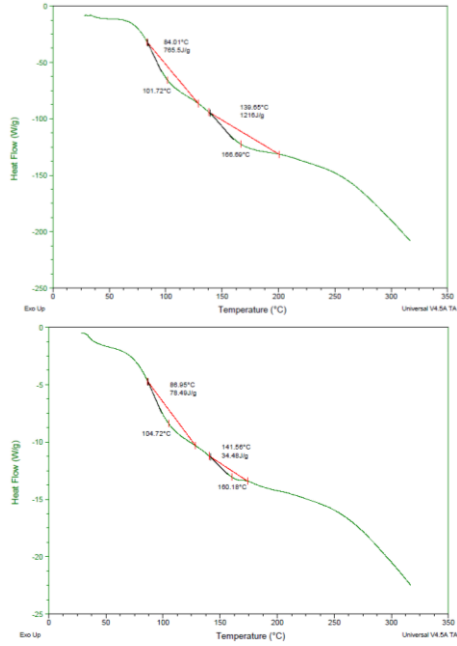


Fig. (3) The charts of the DSC analysis of the six samples.

In Fig. (4), we can observe the changes in the glass transition temperature (Tg) and melting transition temperature (T_m) relative to the varying concentrations of copper and silver weight percent. An outlier case was demonstrated by specimen no. 2, where an additional third downward peak is evident at the lowest temperature onset, which may signify a recrystallization temperature [8]. The ratio of the recrystallization temperature to the pure metals' melting point value typically falls within the range of 0.3-0.4, whereas for organometallic specimen no. 2, the ratio is approximately 0.29. Generally, both T_{g} and T_{m} decrease as the percentage of added silver weight increases during the precipitation process [9]. The intermediate zone between T_g and Tm spans a range of 60°C. The increase in silver weight percentage contributes to the reduction of both T_g and T_m .

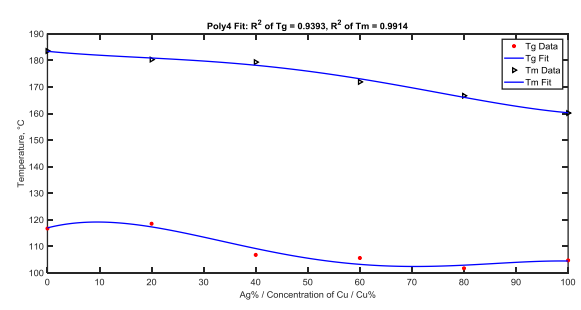


Fig. (4) The variations in the glass transition temperature and the melting transition temperature for the six considered specimens, depending on the weight percentages of copper and silver in their chemical composition

The Differential Scanning Calorimetry (DSC) analysis reveals all potential phase transitions and quantifies the enthalpy change at each transition. As illustrated in Fig. (5), the change in enthalpy during the transformation of all samples from the glassy

phase to the semi-glassy phase at the glass transition temperature ($T_{\rm g}$), and from the semi-glassy phase to the liquid phase at the melting temperature ($T_{\rm m}$), provides valuable insights about the precipitates. Beyond certain temperatures, higher enthalpy differences indicate the energy needed to create the semi-glassy (amorphous) phase. This phase is known for its highly ordered structure, strong bonds, and high stability. In the context of the melting phase at $T_{\rm m}$, a high enthalpy difference suggests that a significant amount of energy is required to break down the bonds and transition the material into the liquid phase [10]. A high enthalpy difference typically indicates greater material stability, as observed in DSC analysis.

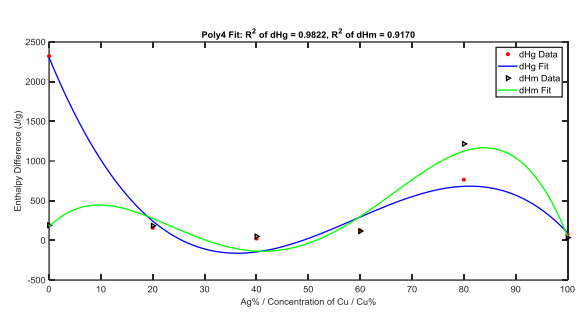


Fig. (5) Enthalpy differences change at glass transition (dHg) and melt transition (dHm) temperatures as a function of weight percent of copper and silver in the specimens

Figure (5) reveals that the enthalpy differences (dHm) associated with the phase transition from the semi-glassy to the liquid phase are relatively similar across all samples. However, it is noteworthy that sample five exhibits the highest dHm value. In the same figure, there is a significant increase in enthalpy difference (dHg) for the phase transition from the glassy to semi-glassy phase for the first specimen. It even surpasses its own dHm value. Sample five also shows an increase in dHg value, although it does not exceed its own dHm value. This difference is characteristic, although pronounced than that of sample one. The remaining specimens show minor variations between their dHm and dHg values. Therefore, it can be inferred that samples one and five have structures of higher stability compared to the other specimens [10].

The FTIR test involved both the well-separated precipitate apart and the supernatant. These products came from the reactants of aqueous salts (CuSO₄.5H₂O, and AgNO₃) solution and the beetroot juice. Therefore, the beetroot juice was used as a control specimen by subjecting it to the same inquiry. The precipitate spectrum in comparison to the reference sample of beetroot juice can be observed in Fig. (6), which showed the transmitted intensities of infrared radiation of wavenumber in between 400 and 4000 cm⁻¹.

The most important recognized chemical groups in beetroot juice [11] are as follows: The peak at 3464 cm⁻¹ corresponds to alcohols and phenols, indicating the presence of O-H bonds stretching

vibration. The absorption peak is commonly associated with chemical groups such as primary and secondary alcohols, as well as phenols, which are aromatic compounds with hydroxyl groups [12].

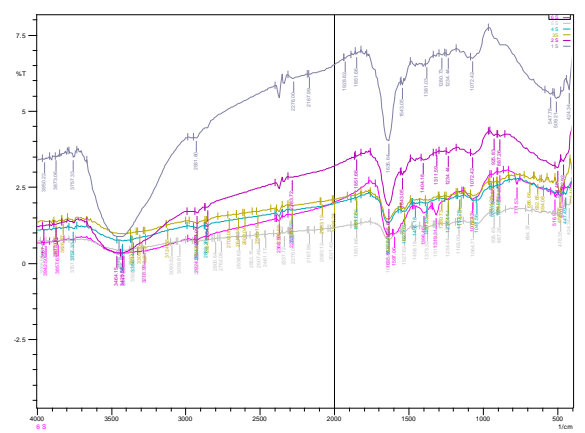


Fig. (6) FTIR chart depicting the spectrum of the precipitate specimens and the control sample, with the dashed curve representing beetroot juice

The broad peak suggests the presence of hydrogen bonding or multiple hydroxyl groups [11]. This broadness decreased as the copper ratio increased. However, the high copper weight percent levels the high transmittance, indicating less sediment interaction with the hydroxyl group. When silver was added, the weight percent of silver was increasing gradually, while that of copper was decreasing. The effect of the two metal components, copper and silver is reversed. The increased broadness and decreased transmittance, mean more deposited hydroxyl with a higher density of hydrogen bonds. However, the precipitated chemical group of O-H did not exceed its concentration in the beetroot juice at the same energy level.

The other prominent wavenumber is 1404 cm⁻¹. This wavenumber corresponds to the medium-O-H bending vibration [11]. The chemical group typically associated with this absorption peak is the carboxylic acid. Carboxylic acids contain the functional group -COOH, which includes an O-H bond. Sample no. 1 showed higher transmittance than the reference at this wavenumber. Conversely, the concentration of the same deposited group in the other samples exceeded that of the beetroot juice. In (IR) spectroscopy, wavenumber range for triple bonds between carbon atoms (C≡C) is typically between 2100 and 2200 cm⁻¹ [11]. This range of absorption bands indicates the stretching vibration in the triple bond shared by two carbon atoms. It is important to note that alkynes, characterized by the presence of C≡C bonds, exhibit absorption in this spectral region. In general, the presence of silver in the samples contributed to a greater increase in absorption at this wavenumber compared to that of the spectrum of the beetroot juice. Flattening of the downward peak may indicate an interaction affecting the chemical

structure of the bond. This could suggest that the element is interacting with the chemical groups associated with that peak, possibly forming new bonds or complexes. This interaction can change the vibrational energy levels, leading to a reduction in the intensity or disappearance of the peak [13].

The C=C stretching vibration of alkenes typically occurs in the range of 1640 to 1680 cm⁻¹ [13]. This band is a characteristic feature of compounds containing carbon-carbon double bonds. The first sample had higher transmittance percentage than the control spectrum, while the second sample had the same transmittance as beetroot juice. Consequently, the transmittance percentage continued to decrease as the silver weight percent increased due to the decrease in the copper percentage.

The absorption peak around 1057 cm⁻¹ is often associated with the C-N stretch in amines. Amines are organic compounds containing nitrogen (N) atoms bonded to carbon (C) atoms. They can be classified as primary (1°), secondary (2°), or tertiary (3°) amines based on the number of carbon substituents attached to the nitrogen atom. The behavior of the transmittance spectrum at this level of energy was generally similar to previous spectra [11,13]. The absorption peak at 501 cm⁻¹ in the FTIR spectrum of beetroot juice corresponds to the C-O stretching vibration of carboxylic acid groups. This peak is related to the stretching motion of the carbon-oxygen (C-O) bonds in carboxylic acids [11]. In general, the transmittance percentages of the samples followed the same order but with lower values.

According to the FTIR chart, it is evident that betalain and anthocyanin, their chemical structure illustrated in Fig. 1, play a significant role in the production and deposition of the metal-organic compound.

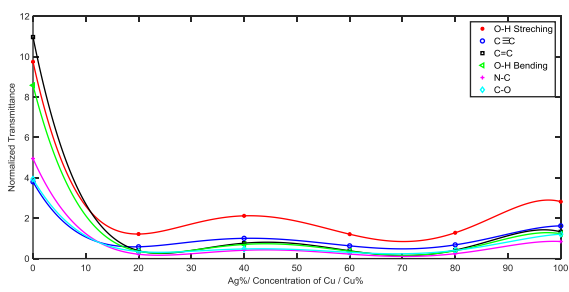


Fig. (7) Changing of the normalized values of the transmittance percentage of the identified chemical groups of the precipitates to that of the beetroot juice, across several variations in the specimens' chemical composition

The potential precipitate type is an organometallic compound. It consists of the interaction of a metallic atom as an acceptor of a pair of electrons (Lewis acid) with the organic part, which acts as a donor (Lewis base). The chemical groups identified and confirmed by the FTIR analysis indicated their presence in the specimens

[14]. The comparison of the normalized transmittance percentage values of the samples to the beetroot juice versus the contents concentrations provides insight into the level of interaction of the metallic ions with the beetroot juice (Fig. 7).

The high transmittance values of the various chemical groups in the 100 wt.% copper sample is evident. The presence of silver in the other samples resulted in increased deposition of all the chemical groups, except for the stretching vibration of the hydroxyl group, which was relatively low in all samples. The FTIR test is based on the Beer-Lambert law, where high transmittance indicates low absorbance of the sample. On the other hand, the FTIR chart of the supernatant shows the same chemical groups as the precipitate, but at lower concentrations, especially in the rich-copper samples, as depicted in Fig. (8). Overall, the concentration of residual chemical groups in the supernatant is somewhat lower than that of the beetroot juice, as shown in Fig. (9).

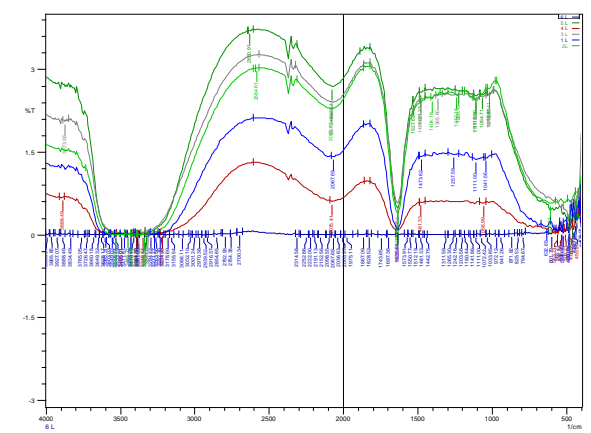


Fig. (8) FTIR chart of all specimens' supernatant shows the transmittance percent of all samples with that of the control sample of the beetroot juice versus the wavenumber

Figures (7) and (9), displayed inverse values about the normalized transmittance versus the concentration of the samples. Specifically, a concentration of 0%, 40%, and 100% for Cu represented maxima for the precipitate but minima for the supernatant and vice versa for the other values of the concentration. The behavior represents the integral relationship between the precipitate and the supernatant.

The data presented in Fig. (10) demonstrated notable differences in absorbance values, particularly in the first and sixth samples, with the most significant variation observed in the last sample. It is interesting to observe that despite its shorter range compared to visible wavelength, the UV absorbance is higher. This suggests the presence of aromatic compounds with extended π -electron systems, Known to absorb UV light, rather than extended conjugated groups in the obtained precipitate, which absorb visible light [15].

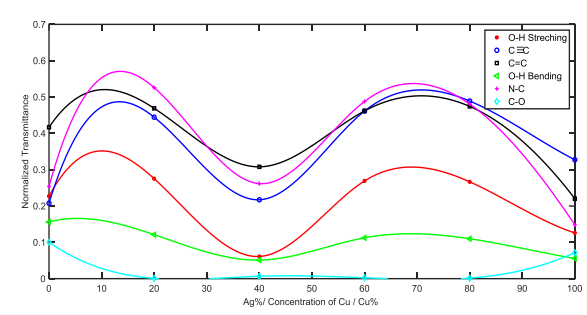


Fig. (9) The alteration of the normalized values of the transmittance percent of the different chemical composition of the samples' supernatant to that of the beetroot juice

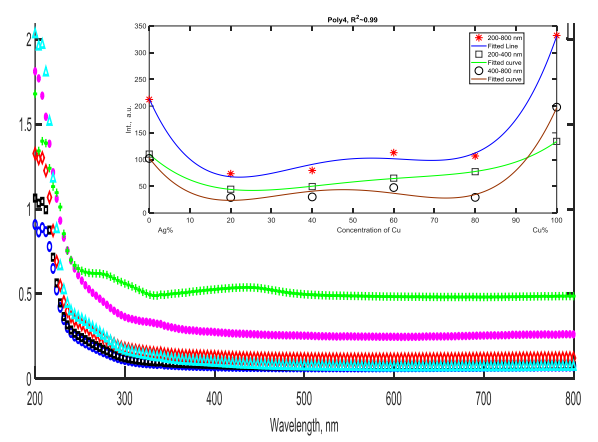
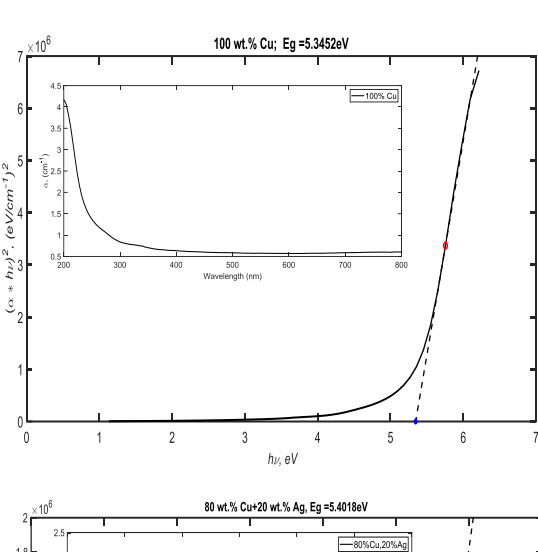
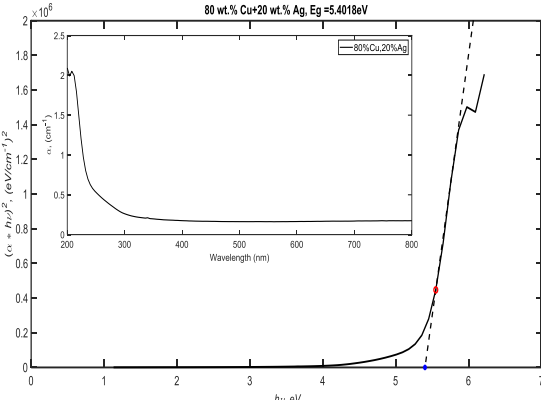


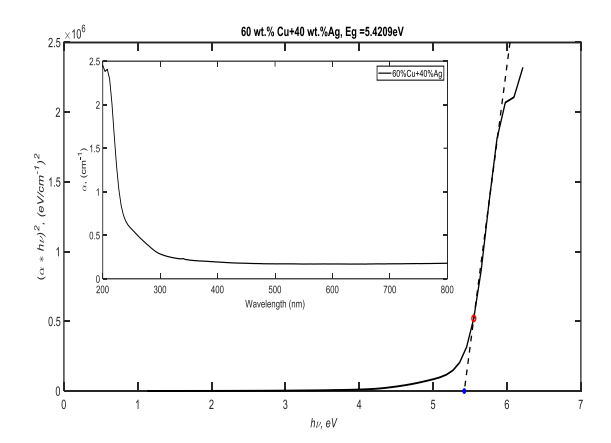
Fig. (10) Absorption spectra of the six specimens with different concentrations

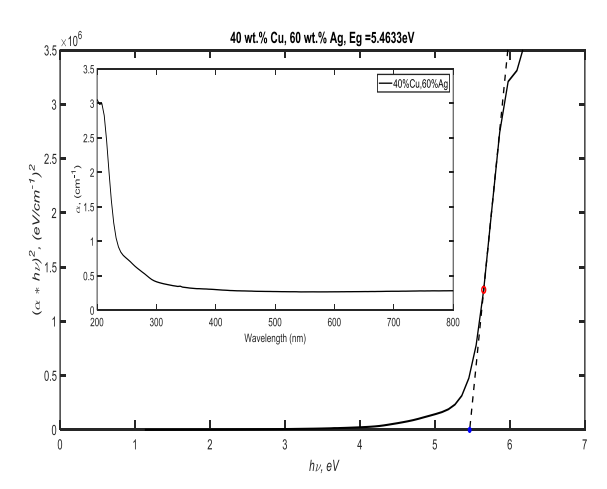
Betalains exhibit interesting behavior when it comes to absorbing light. Specifically, betaxanthins, a type of betalain, absorb visible light with a maximum peak of around 475 nm. This absorption can be measured using UV-visible spectroscopy. Betalains absorb light in the UV region as well. Their chromophore, the part responsible for color, elevates π -electrons to higher energy levels (π *). This increased reactivity results from a drop in activation energy due to UV absorption [2], obviously for sample six of the highest sediment of betalain.

The experimental data from the UV-Visible measurements of the sediment specimens were used to calculate their absorption coefficients. These calculations are crucial for determining the band gap values, which are illustrated in Fig. (11). This figure represents the indirect allowed electronic transition as per the appropriate Tauc plot. The band gap of a material represents the energy difference between the top of the valence band and the bottom of the conduction band. This energy difference is essential in determining the material's electronic and optical properties.









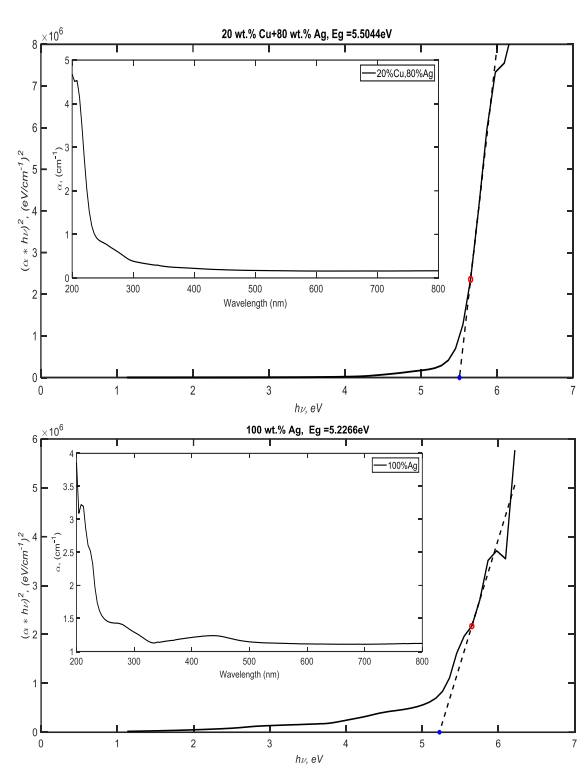


Fig. (11) The determination of the band gap for the six samples and their absorption coefficient versus wavelength is important

Changes in the chemical composition of a material can impact the band gap through various influential factors, including atomic structure and bonding, elemental composition, lattice parameters, impurities and defects, and quantum confinement. The band gap values changed according to the variations in chemical composition [16], as depicted in Fig. (12).

Although the minimum value of the band gap of the first sample of the pure metal copper-organic compound, the band gap increases as the copper content approaches zero and the silver content approaches 100 percent due to various factors. One potential explanation is that the material's electronic structure is highly influenced by the specific elements present and their arrangement. Transitioning from a composition with both copper and silver to one that is predominantly silver could potentially alter the energy levels and electronic interactions within the material, causing a change in the band gap. Additionally, the varying atomic sizes, electro negativities, and bonding characteristics of copper and silver may influence the material's overall electronic properties [17].

The composition at which the band gap reaches its maximum value is just before reaching 100% Ag content. This happens because of the specific atomic configurations and interactions among the elements in the material. In this composition, the electronic structure is organized in a way that maximizes the band gap. However, increasing the Ag content beyond this point leads to changes in the electronic structure that cause a steep decrease in the band gap.

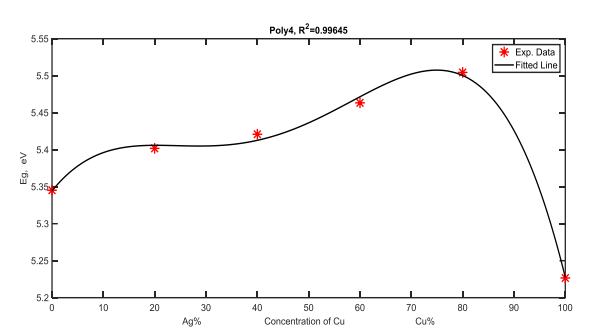


Fig. (12) Band gap values of the different chemical composition six samples of the precipitate versus the concentration of copper

The extinction coefficient is the ability of a material to absorb or attenuate the incident radiation on it. It depends on the path length, the concentration, and the absorbance of the material. The results of the extinction coefficient of the sediments' samples are shown in Fig. (13). The extinction rates are higher in visible light than in the UV-radiation range, especially for the sixth, first, and fourth samples, respectively. The other samples showed no distinctive difference between the influence of visible light and UV radiation on the extinction values. The effect of the chemical composition appeared clearly in Fig. (14).

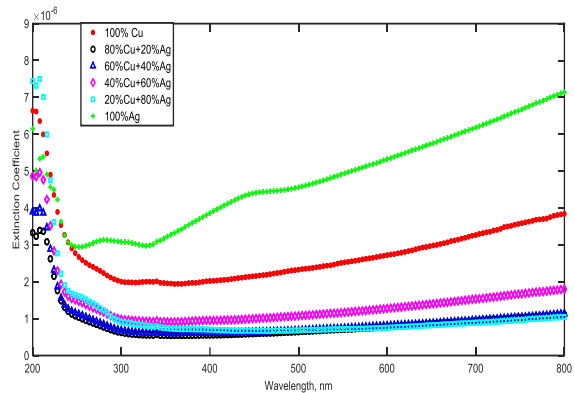


Fig. (13) The extinction values of the six samples change according to the wavelength

The measured reflectance of the precipitates consistently showed high values, indicating strong reflective properties. The reflectance curves have an inverted shape compared to the absorbance at different wavelengths, as shown in Fig. (15), and the varied metal concentrations are clearly illustrated in Fig. (16). The general behavior agreed with the band gap values. A smaller energy gap corresponds to lower reflectivity [18].

The reflectance value has a key role in counting the refractive index. The behavior of the refractive index belonging to the precipitates' samples is shown in Fig. (17). The fascinating results showed negative values of all the samples, which indicate metamaterial [19]. The sixth sample had the highest negative values of the refractive index versus the

variable of wavelength. The first sample of pure copper added within the precipitate exhibited higher negative values of the refractive index than the values of the other samples by a little difference. The influenced refractive index of the samples by their chemical composition at the visible light and ultraviolet radiation is shown obviously in Fig. (18). Despite the component of visible light being more effective than that of the UV radiation, the sixth and first samples appeared higher negative values at the UV range than that of the visible light.

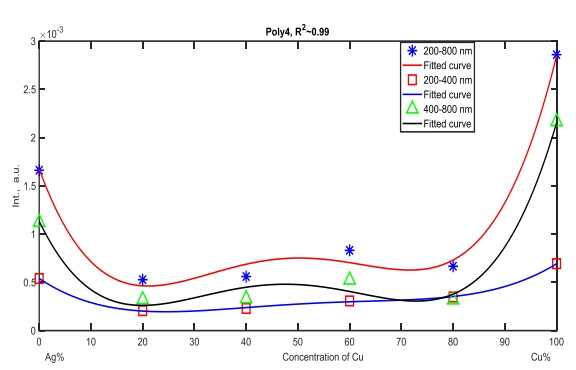


Fig. (14) The integrated area of the extinction coefficient to the added metal concentration. The values of the extinction coefficient are associated with the purity of the metals present in the sample and the small size of the band gap value

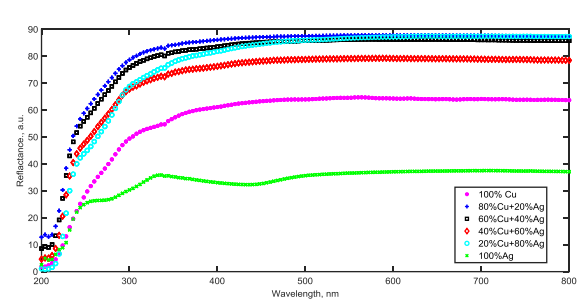


Fig. (15) The reflectance values versus the wavelengths for the precipitate samples

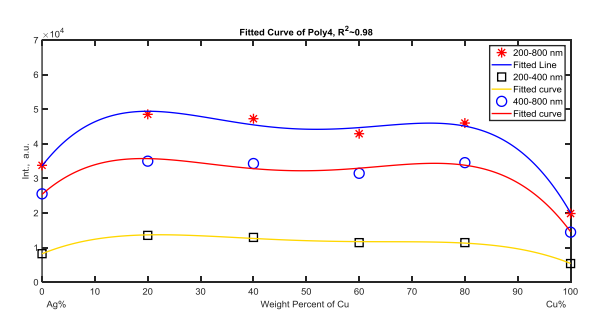


Fig. (16) The relationship between the integrated reflectance intensity values and the concentration of the samples

When the refractive index is positive, light bends toward the normal upon entering the material, composed of naturally occurring materials. In the realm of the Negative Refractive Index of the metamaterials (NIMs), something remarkable happens. Light bends away from the normal by skillfully manipulating the electric permittivity (ϵ) and magnetic permeability (μ) properties [19].

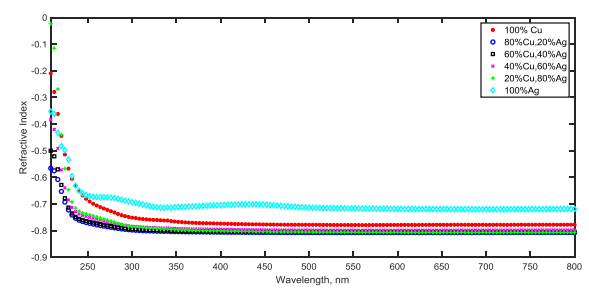


Fig. (17) The negative range of the refractive index for the different samples as a function of wavelength

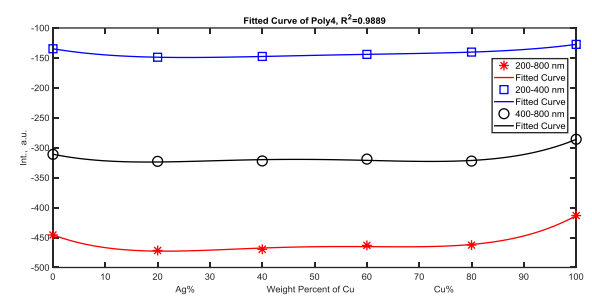


Fig. (18) The variation of the integrated area of the refractive index according to the chemical composition alteration of the samples for the ranges of visible light and UV radiation

The structure of negative-index metamaterials (NIMs) consists of tiny building blocks called periodic unit cells, much smaller than the wavelength of the electromagnetic radiation they interact with. These unit cells are arranged in patterns to form the NIM structure, resulting in properties beyond their constituent materials. For the negative-index metamaterials, light bends away from the normal, and their refractive index is negative. NIMs exhibit optical behavior that challenges traditional understanding [19].

The behavior of the real electric permittivity, shown in Fig. (19), is the electric permittivity changing by the wavelength with low values. When ϵ_1 is positive, it indicates that the material supports electric field propagation [20]. The lowest value is that of the sixth sample and comes after it the electric permittivity of the first sample, which is less than the other by a tiny difference, is. In another aspect, the effect of the wavelength and the chemical composition of the samples seem more obvious in Fig. (20).

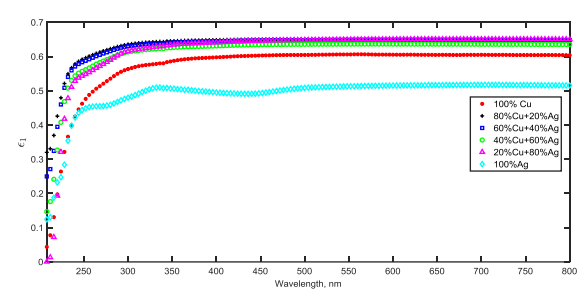


Fig. (19) The change of the real electric permittivity values of the precipitates samples of different chemical compositions against the wavelength

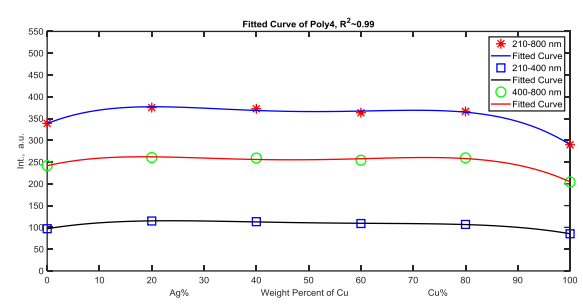


Fig. (20) The positive integrated values of the real electric permittivity change with the varying weight percent of copper and silver in the precipitates' chemical composition

The behavior can be directly attributed to the low values of the extinction coefficient of the samples. In contrast, the calculated imaginary electric permittivity revealed intriguing negative values across all samples in the 200-800 nm wavelength range as shown in Fig. (21). The negative value of the imaginary electric permittivity ϵ_2 refers to supporting of the absorption the energy from the electric field. Figure (22) shows the relationship between the integrated values of the negative imaginary permittivity and the concentration of the Cu and Ag in the samples of the precipitate [21].

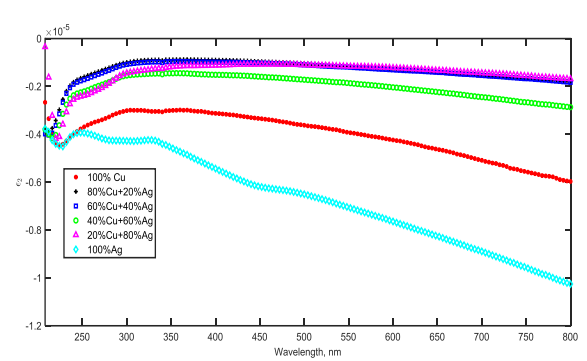


Fig. (21) The change in the imaginary electric permittivity over a small range versus the wavelength

The behavior of the optical conductivity of the precipitate's samples is shown in Fig. (23). The obtained fascinating negative values of the optical conductivity are due to the negative values of the refractive index.

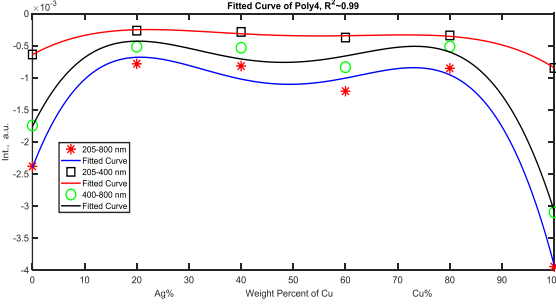


Fig. (22) The contributions of visible light, UV radiation, and the integrated values of negative electric permittivity versus the concentration of copper and silver in the samples

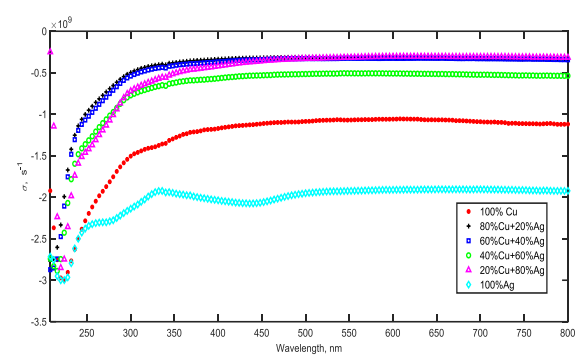


Fig. (23) The negative optical conductivity related to the wavenumber

The lowest values are sorted according to the order of the sixth, first, fourth, and other samples. Fig. (24) shows the change of the negative integrated values of the optical conductivity versus the variant values of the concentration of metals of the precipitate samples. The equivalence of the copper and silver content in the samples appeared the same effect of the negative optical conductivity at both UV and visible light. However, the more divergence of the quantity of the two metals, the more different the influence of the negative optical conductivity in accordance to the type of the wavelength range.

Optical conductivity is a property of materials that describes the relationship between the induced current density and the magnitude of the induced electric field for arbitrary frequencies. The optical conductivity is closely related to the dielectric function, which generalizes the dielectric constant to arbitrary frequencies [22].

Negative optical conductivity is when a material's conductivity decreases upon illumination. Typically, illumination leads to the generation of additional carriers, thus increasing the material's conductivity. This is known as photoconductivity (PPC). However, some materials opposite behavior, decreasing conductivity when exposed to light. phenomenon is called negative photoconductivity (NPC). Exposure to light causes a metastable reduction in photoconductivity. Defects, impurities, and recombination centers can influence negative photoconductivity. In some cases, carriers captured in traps exhibit persistent photoconductivity. Furthermore, deep impurities with significant lattice relaxation may also exhibit small recombination cross-sections [22].

The negative photoconductivity observed in the precipitate could result from the trap states. Carriers trapped in defects or impurities reduce overall conductivity. Moreover, the slow recombination centers hinder carrier recombination, leading to persistent effects. Likewise, carriers may shift from slow to fast recombination centers under certain conditions, affecting conductivity.

Fig. (24) The proportionality of the negative values of the optical conductivity with the weight percent of the copper and silver in the samples of the precipitate

Cu%

4. Conclusion

The concentration of silver ions compared to copper during the deposition process affects material properties. Pure copper has the highest stability, but pure silver exhibits the best optical properties. Sample six, with pure silver, shows the lowest band gap, reflectance, and optical conductivity. The negative values suggest potential metamaterial behavior due to the production of fine structures.

Acknowledgements

Special words of thanks to Prof. Ahmed Hashim, Prof. Majeed A. Habeeb, and Ms. Saja, Physics Department, College of Education for Pure Science, University of Babylon.

References

- [1] S. Kulkarni and A. Mishra, "Metamaterials: Advancement and Futuristic Design Approach", Wireless Personal Commun., 124 (2022) 2075-2095.
- [2] E. A. Hussain, Z. Sadiq and M. Zia-Ul-Haq, "Chemistry of Betalains, In: **Betalains:** Biomolecular Aspects", Springer (2018), Ch. 1, p.
- [3] H. Arslanoglu and F. Tumen, "A study on cations and color removal from thin sugar juice by modified sugar beet pulp", J. Food Sci. Technol., 49 (2012) 319-327.
- [4] A. Sharma, H. Singh and A. Gupta, "A Review Analysis of Metamaterial-Based Absorbers and Their Applications", J. Superconduct. Novel Magnet., 35 (2022) 3067-3083.
- [5] E. Ghanbari, S.J. Picken and J.H. van Esch, "Analysis of differential scanning calorimetry (DSC): determining the transition temperatures, and and heat capacity changes multicomponent systems by analytical model fitting", J. Therm. Anal. Calorim., 148 (2023) 12393-12409.
- [6] A.G. Al Lafi, A. Alzier and A.W. Allaf, "Twodimensional FTIR spectroscopic analysis of crystallization in cross-linked poly(ether ether ketone)", Int. J. Plast. Technol., 24 (2020) 1-8.
- [7] P. Kaur, M. Singh and P. Birwal, "Differential Scanning Calorimetry (DSC) for the Measurement of Food Thermal Characteristics and Its Relation to Composition and Structure", in: Techniques to

Measure Food Safety and Quality, eds. M.S. Khan and M. Shafiur Rahman, Springer (2021). Ch. 13, p. 283.

Vol. 20, No. 4, October-December 2024, pp. 843-852

- [8] S. Solhjoo and R. Ebrahimi, "Prediction of norecrystallization temperature by simulation of multipass flow stress curves from single-pass curves", J. Mater. Sci., 45 (2010) 5960-5966.
- [9] K. Xue et al., "Hot Deformation Behavior and Dynamic Recrystallization Mechanism of Fe-18.2Mn-0.52C Twinning-Induced Plasticity Steel", J. Mater., 13 (2024) 1-15.
- [10] M.E. Glicksman, "Thermodynamics of Crystal-Melt Phase Change", in: Principles of Solidification, Springer (NY, 2011), Ch. 2, pp. 27-51.
- [11] H.N. Murthy, K.Y. Paek and S.Y. Park, "Bioactive Compounds in the Storage Organs of Plants", Springer Nature (2024), Part VI, p. 843.
- [12] D.L. Pavia, G. M. Lampman, G. S. Kriz, & J. R. Vyvyan, "Introduction to Spectroscopy", Cengage Learning (2008), Ch. 2, p. 14.
- [13] T. Hasegawa, "Fundamentals of FT-IR", in: Infrared Ouantitative Spectroscopy Understanding of a Condensed Matter, Springer (Tokyo, 2017), Ch. 1, pp. 1-37.
- [14] J. Romanova et al., "Molecular Design of Materials: Effect of the Organometallic Metallophilic Interactions, Ligand, Metal, and Oxidation State", in: Quantum Systems in Physics, Chemistry, and Biology, eds. A. Tadjer, R. Pavlov, J. Maruani, E. Brändas, & G. Delgado-Barrio, Progress in Theoretical Chemistry and Physics, vol. 30, Springer, Cham (2017), Part 2, pp. 139-158.
- [15] O.L. Pavlenko et al., "Electron Structure and Optical Properties of Conjugated Systems in Solutions", in: Modern Problems of the Physics of Liquid Systems, eds. L. Bulavin & L. Xu, PLMMP 2018, Springer Proceedings in Physics, vol. 223, Springer, Cham (2019), Part 3, pp. 225-248.
- [16] H.H. Perkampus, "Evaluation of UV-VIS Spectral Bands", in: UV-VIS Spectroscopy and Its Applications, Springer Lab Manuals, Springer, Berlin, Heidelberg (1992), Ch. 2, pp. 215-234.
- [17] M. Goyal, "Impact of alloying on the bandgap energy in nano-sized ternary semiconducting compounds", J. Computat. Electron., 23(1) (2024) 12-21.
- [18] P.S. Reddy, B.S. Raghavendra and A.V. Narasimhadhan, "Approximate Finite Rate of Innovation Based Seismic Reflectivity Estimation", Circuits Syst. Signal Process., 1(23) (2024) 1-16.
- W. Cai and V. Shalaev, "Negative-Index Metamaterials", in: Optical Metamaterials, Springer (NY, 2010), Ch. 6, pp. 101-122.
- [20] J. Zhang et al., "Electric-field-enhanced permittivity dependence on temperature and cooling rate", Appl. Phys. A, 127 (2021) 386.
- [21] Z. Leng et al., "Progress in percolative composites with negative permittivity for applications in electromagnetic interference shielding capacitors", Adv. Compos. Hybrid Mater., 6 (2023) 195.
- [22] J. Mistrik et al., "Optical Properties of Electronic Materials: Fundamentals and Characterization", in: Springer Handbook of Electronic and Photonic Materials, eds. S. Kasap & P. Capper, Springer Handbooks, Cham (2017), Ch. 3, pp. 47-82.